UNIVERSITY OF CALIFORNIA
RIVERSIDE

MEASUREMENT OF THE LONGTIDUDIANL SINGLE SPIN ASYMMETRY, A_L, FOR POLARIZED PROTON-PROTON COLLISIONS IN THE $W \to \mu$ DECAY CHANNEL

A Dissertation submitted in partial satisfaction
of the requirements for the degree of

Doctor of Philosophy

in

Physics

by

Michael J. Beaumier

August 2016

Dissertation Committee:

Professor Kenneth Barish , Chairperson
Professor Rich Seto
Professor John Ellison

The Dissertation of Michael J. Beaumier is approved:

Committee Chairperson

University of California, Riverside

Acknowledgments

In no particular order now, but say something nice about each person.

Advisors and Mentors

Ken Barish, Richard Hollis, K. Oleg Eyser, Ralf Seidl, Francesca Giordano, Joe Seele, Josh Perry, Martin Leitgab, Chris Pinkenburg, Martin Purschke, Collaborators, Sangwha Park, Daniel Jumper, Abraham Meles, Chong Kim,

Friends and Family

Bob Beaumier, Marian Beaumier, Joe Beaumier, David Beaumier, Emily Vance, Jackie Hubbard, Alexander Anderson-Natalie, Corey Kownacki, Chris Heidt, Pat Odenthal, Behnam Darvish Sarvestani, Oleg Martynov,

Some say that it takes a village to raise a child. The same can be said of raising a graduate student up to earning a PhD. This thesis is dedicated to the multitude who have helped me become the man I am today, and to students who struggle, and their mentors who do not give up on them.

ABSTRACT OF THE DISSERTATION

MEASUREMENT OF THE LONGTIDUDIANL SINGLE SPIN ASYMMETRY, A_L, FOR POLARIZED PROTON-PROTON COLLISIONS IN THE $W \to \mu$ DECAY CHANNEL

by

Michael J. Beaumier

Doctor of Philosophy, Graduate Program in Physics
University of California, Riverside, August 2016
Professor Kenneth Barish , Chairperson

This thesis discusses the process of extracting information about the spin structure of protons, specifically, spin contributions from the sea of quarks and antiquarks, which are kinematically distinct from the 'valence quarks'. We have known since the 'proton-spin crisis' [3] of the 1990s that proton spin does not entirely reside in the valence quarks, so the thurst of experimental efforts since then have been designed to determine both how to probe the proton spin structure, and how to validate models for proton spin structure. Here, I discuss one particular approach to understanding the sea-quark spin contribution, which utilizes the production of real W-bosons, and the W coupling with polarized spin structure in the proton sea, as produced from polarized protons collisions. Only one of the colliding protons is longitudinally spin polarized, in this analysis, and they are collided at an energy of $500GeV$. The expermental observable used is referred to as "A_L" which is expressed mathematically as a ratio of sums and differences of various helicity combinations of singly polarized interactions between two protons, i.e. $p + p^{\Rightarrow} :\to W \to \mu + \nu$. Once A_L has been experimentally measured, it can then be used to determine appropriate polarizations of proton sea-quarks, within a given uncertainty, if we write the cross-sections used in the calculation of A_L in terms of polarized parton distribution functions. Finally, this thesis will also include a discussion of my work experimentally determining the absolute luminosity of collisions at RHIC, which is needed as a normalization on any cross section used in the analysis. In particular, studying the cross section of the W interaction can help to validate our models for assigning a signal-to-background ratio to the $W \to \mu$ events.

Contents

List of Figures

List of Tables

Chapter 1

Introduction

1.1 A Brief History of the Proton

The angular momentum of the proton has been a subject of study for the last 20 years[CITATION NEEDED]. One of the challenges of particle physics is to create a framework which can accurately describe matter, as well as predict the behavior of matter at all energy scales. The proton is a baryon which makes up the majority of the mass in the visible universe, yet fully understanding the origins of its properties - such as its mass and spin, still eludes us. However, through the applicaiton of the scientific method over many generations of physicists, we have magnificently described this important particle, and understood much of its properties. However, one property which still defies our descriptions is its fundamental angular momentum, spin.

Our understanding of the proton has evolved and sharpened since the first experiments in deep inelastic scattering showed that the proton is not a fundamental particle [4]. Gell-Mann later planted the seeds of a theoretical framework which could in part describe some of the structure of baryons, a class of hadrons which we may naively describe as composed of three 'valence quarks'[CITATION NEEDED]. We can apply well known spin-sum rules to the indivdual spins of the valence quarks which compose the proton in our naive valence-model to produce a correct prediction for the protons' spin $\frac{1}{2}$. When experimenters set out to measure the contribution of these valence quarks in 1988 at the EMC experiment [3], they were flabbergasted to find that the valence quarks carry only a small fraction of the proton's spin. Although recent papers [10] suggest that this 'spin crisis' is

simple due to misattribution of spin, most literature to date has focused on understanding how to model the proton with parton distribution functions. These parton distribution functions come in many varieties, and probe different degrees of freedom within the proton, in both the case of unpolarized partion distribution funcitons, and polarized parton distribution functions.

1.2 Scope and Objectives of This Work

This thesis will describe the research I carried out between May of 2010 through August of 2016. I will

Chapter 2

Physics Background

2.1 How to Model Proton Spin

2.2 How to Measure Proton Spin

2.2.1 A Brief Description of Fixed Target Experiments

2.2.2 A Brief Description of Collider Experiments

2.3 How to Measure Beam Luminosity in Collider Experiments

Chapter 3

Experimental Apparatus

3.1 The Relativistic Heavy Ion Collider

3.1.1 Overview

3.1.2 Production of Polarized Proton Beams

3.2 The Pioneering High Energy Nuclear Interaction Experiment

3.2.1 Data Collection

3.2.2 The DAQ

3.2.3 Physics Triggers

Trigger 1

Trigger 2

Trigger 3

Trigger 4

3.2.4 Muon Trigger Upgrade

Chapter 4

Data Cleaning

4.1 Overview

Now that we have discussed the various aparatuses provided by the PHENIX experiment, we can go into more depth with the process of engineering features. For this analysis, we consider only events which are identified by the Muon Arms subsystem as being muons. The raw data provided by PHENIX is quite complex, and at the hardware level is generally not too useful for physics analysis.

In this chapter, we will discuss the process of cleaning our data set, the goal of which is to get rid of background data, while keeping any event that could possibly contribute to the $W \rightarrow \mu$ signal. This cleaning is done in three stages. The first stage concerns applying a simple basic cut to our data set to remove events which are kinematically forbidden from having W boson parent particles, this is called the "Basic Cut".

After this, we label data with W_{ness}, which is an event's likelihood for coming from a W boson decay. Although this is part of data cleaning, since W_{ness} is an important parameter in the analysis, it is discussed in Section **??**.

Finally, we must estimate the overall yield of μ resulting from the various proton helicity combinations, and the signal to background ratio characterizing that yield. Again, since this is also an important part of the physics, it is discussed in Section 5.2.6.

4.2 Analysis Variables and the Basic Cut

A brief summary of the kinematic variables used later in the analysis is given in Table 4.1. In addition four sets of RPC cluster variables exist which are being used as main RPC variables during run12 and after. Those contain projections from either vertex, Station 1, 3 or the MuID road to the corresponding z positions of the RPCs based on the tracks in the PHMuoTracksOut node and are directly taken over from the RpcMuoTracks node in the dsts:

- newsngmuons→Branch("RpcMatchVtx",0,"Rpc3dca[_RecoTracks]/F:
  Rpc3time[_RecoTracks]/F:Rpc3x[_RecoTracks]/F:Rpc3y[_RecoTracks]/F:
  Rpc1dca[_RecoTracks]/F:Rpc1time[_RecoTracks]/F:Rpc1x[_RecoTracks/F:
  Rpc1y[_RecoTracks]/F");

- newsngmuons→Branch("RpcMatchSt1",0,"Rpc3dca[_RecoTracks]/F:
  Rpc3time[_RecoTracks]/F:Rpc3x[_RecoTracks]/F:Rpc3y[_RecoTracks]/F:
  Rpc1dca[_RecoTracks]/F:Rpc1time[_RecoTracks]/F:Rpc1x[_RecoTracks]/F:
  Rpc1y[_RecoTracks]/F");

- newsngmuons→Branch("RpcMatchSt3",0,"Rpc3dca[_RecoTracks]/F:
  Rpc3time[_RecoTracks]/F:Rpc3x[_RecoTracks]/F:Rpc3y[_RecoTracks]/F:
  Rpc1dca[_RecoTracks]/F:Rpc1time[_RecoTracks]/F:Rpc1x[_RecoTracks]/F:
  Rpc1y[_RecoTracks]/F");

- newsngmuons→Branch("RpcMatchMuID",0,"Rpc3dca[_RecoTracks]/F:
  Rpc3time[_RecoTracks]/F:Rpc3x[_RecoTracks]/F:Rpc3y[_RecoTracks]/F:
  Rpc1dca[_RecoTracks]/F:Rpc1time[_RecoTracks]/F:Rpc1x[_RecoTracks]/F:
  Rpc1y[_RecoTracks]/F");

For the moment the timing and DCA distributions we use are those matching from station 1 for RPC1 and from station3 for RPC3. In addition, in order to improve the background rejection in the FVTX acceptance, for this analysis several new variables are added in relation to the FVTX-MuTr matching which were directly taken over from the corresponding methods in the PHMuoTracksOut node. Those are fvtx_dr, fvtx_dϕ and fvtx_dθ which compare the FVTX tracklets radial position, azimuthal and polar angles with

Table 4.1: Definition of the main kinematic variables used in this analysis.

$DG0$:	distance between the projected MuTr track and the MuID road at the gap 0 z position in cm.
$DDG0$:	deviation of the slopes of the MuTr track and the MuID road at the gap 0 z position in degrees.
$DG4$:	distance between MuTr track and MuID road at the gap 4 z position in cm[1].
χ^2:	Track fit quality which describes the quality of the fit to the MuTr and MuID hits. Note, that due to the amount of noise hits in the MuTr it cannot be directly compared to a statistical χ^2 distribution.
DCA_z:	closest distance of approach to the vertex position as extracted using the BBC after projecting the muon track back towards the vertex position. This DCA is the absolute difference of the z positions of vertex and projected track in cm.
DCA_r:	closest distance of approach to the vertex position as extracted using the BBC after projecting the muon track back towards the vertex position. This DCA is the absolute difference of the radius of the projected track in cm.
$\Delta\phi_{12}$:	Azimuthal angle difference between between the MuTr stations 1 and 2 in radians.
$\Delta\phi_{23}$:	Azimuthal angle difference between between the MuTr stations 2 and 3 in radians.
$RpcDCA$:	transverse distance between the muon tracks' position projected on to the RPC3 z position and the closest RPC hit cluster in cm.
$RpcTime$:	Absolute difference between the RPC hit time and the optimal time for collision related particles in bins of the RPC TDCs (106 ns/44)
$mult$:	Multiplicity variable based on 4∗(#Number of other tracks in same arm) + (#Number of tracks in other arm)
$FVTX_{d\phi}$:	Phi residual between MuTr and FVTX track

those of the MuTr as an extrapolated z position between the two. Another FVTX related addition is the FVTX hit multiplicity within a cone of INPUT RANGE HERE around the projected track. This varible will henceforth be called FVTX_cone.

The "Basic Cut" is defined:

- Last MuID gap has to be gap 4 to ensure muons penetrating through all MuID steel
- maximum momentum p<250 GeV/c which is the maximum possible physical energy
- χ^2<20 to require only reasonable tracks
- $DG0$<20 cm.
- $DDG0$<9 degrees.
- single muon candiate in event.

In this W analysis one is interested in removing most lower momentum particles which originate predominantly from background processes while keeping most of the W decay muons. With the above cuts, we aim to reduce part of the fake muons background assuring a good muon track reconstruction ($DG0$,$DDG0$ and χ^2 cuts) and selecting tracks with momentum smaller than the maximum possible physical energy. After applying these basic cuts, the background will be further reduced via a likelihood method, described in chapter **??**, where background and signal features will be studied in detailed.

The correlations between the several cut variables are shown in Fig. 5.2 for data and for the W-si The only exception is the correlation between the vertex extrapolated variables DCA_z and DCA_r and the FVTX related matching variables. This is not entirely unexpected as both should be sensitive to the amount of multiple scattering in the central magnet yoke and initial shielding.

4.3 Feature Engineering

4.3.1 Discriminating Kinematic Variables

4.3.2 Simulations

Chapter 5

Spin Analysis

5.1 Classification of Signal or Background Events

After producing our data set, engineering features which help us convert our experimental data into observables, we are then tasked with the problem of separating out signal events from background events. Many processes are capable of producing muons, many of which are dominant in the W boson kinematic regime (Figure 5.1).

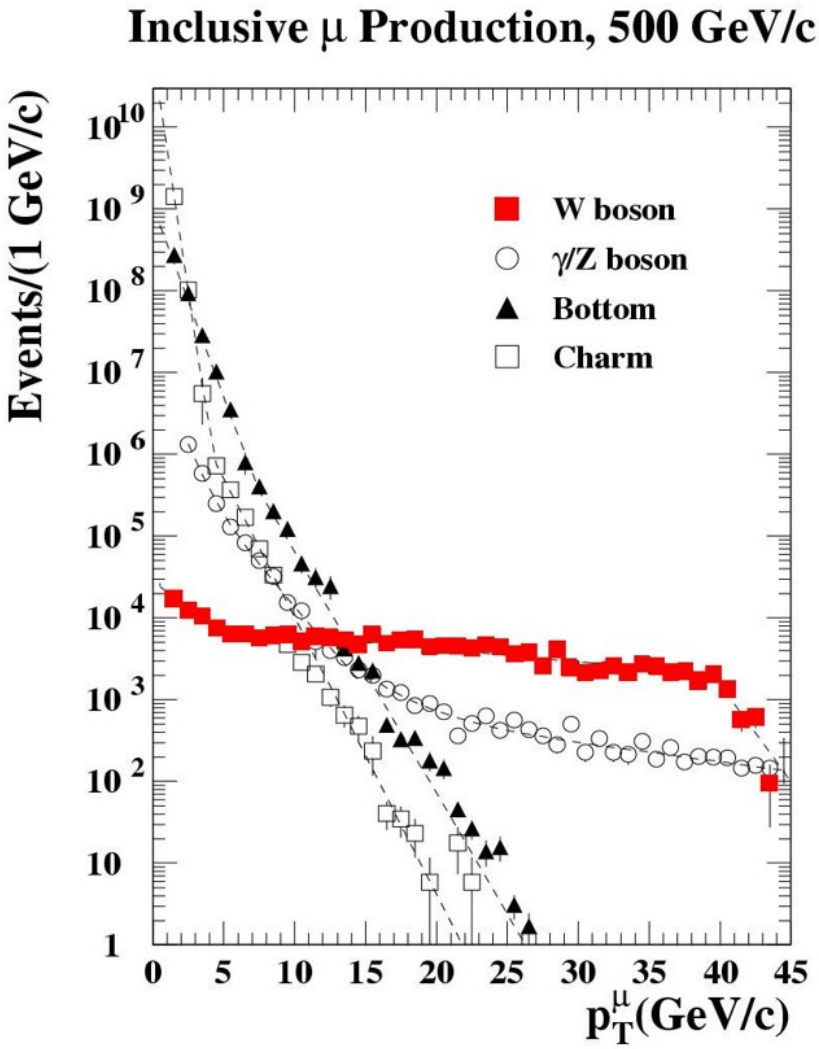

Figure 5.1: Observing the production of muon as a function of p_T, we can see that in the kinematic region of W production that the dominant sources of muons come from other processes. The new PHENIX muon trigger threshold is sensitive at 10 GeV/c and above.

We can divide up the total observed muon spectrum into contributions from three sources:

- Real Muon Background
  - Z,γ^*
  - $W \rightarrow$had

  - $W \rightarrow$tau
  - onium
  - open charm
  - direct photon
- Fake Muons (Hadronic Background)
  - Hadrons which are reconstructed as high p_T muons due to detector resolution.
- Signal Muons
  - Real $W \rightarrow \mu$ events.

Previous analyses have attempted to separate the muon spectrum into p_T bins, to estimate the composition, however, because the $W \rightarrow \mu$ signal is so small in the forward kinematic regime, these methods are not sufficient, as there is no 'visible' cutoff in the spectrum. However, by using simulations. However, we may use other methods to split up our spectrum, with the ultimate goal of calculating A_L, and correcting for background dilution using the signal to background ratio. We must use another method to effectively describe the difference between an event which comes from a signal, vs background event.

5.1.1 Naive Bayes Classification

There are many techniques available for classifying a collection of variables (a feature set) into categories. Naive Bayes classification is an excellent candidate for classification, in cases where we have two classifications with distributions of featuresets which are uncorrelated. Naive Bayes even works when feature sets are slightly correlated. It is a robust, fast, scalable machine learning technique. Traditionally used for classification of text documents, Naive Bayes is also able to handle numeric features whose distributions are known [5].

In our analysis, we begin with a Naive Bayes classifer which is trained to classify two signal muons, vs background muons. We combine both Real Muon Background muons and Fake Muons (Hadronic Background Muons) in the label of "Background Muons" at this stage, though, later, we will separate out the muons further.

The descriniating variables described in 4 were chosen from the multitude of possible physical event parameters, because they were all maximally uncorrelated. Concretely, these correlations are presented in

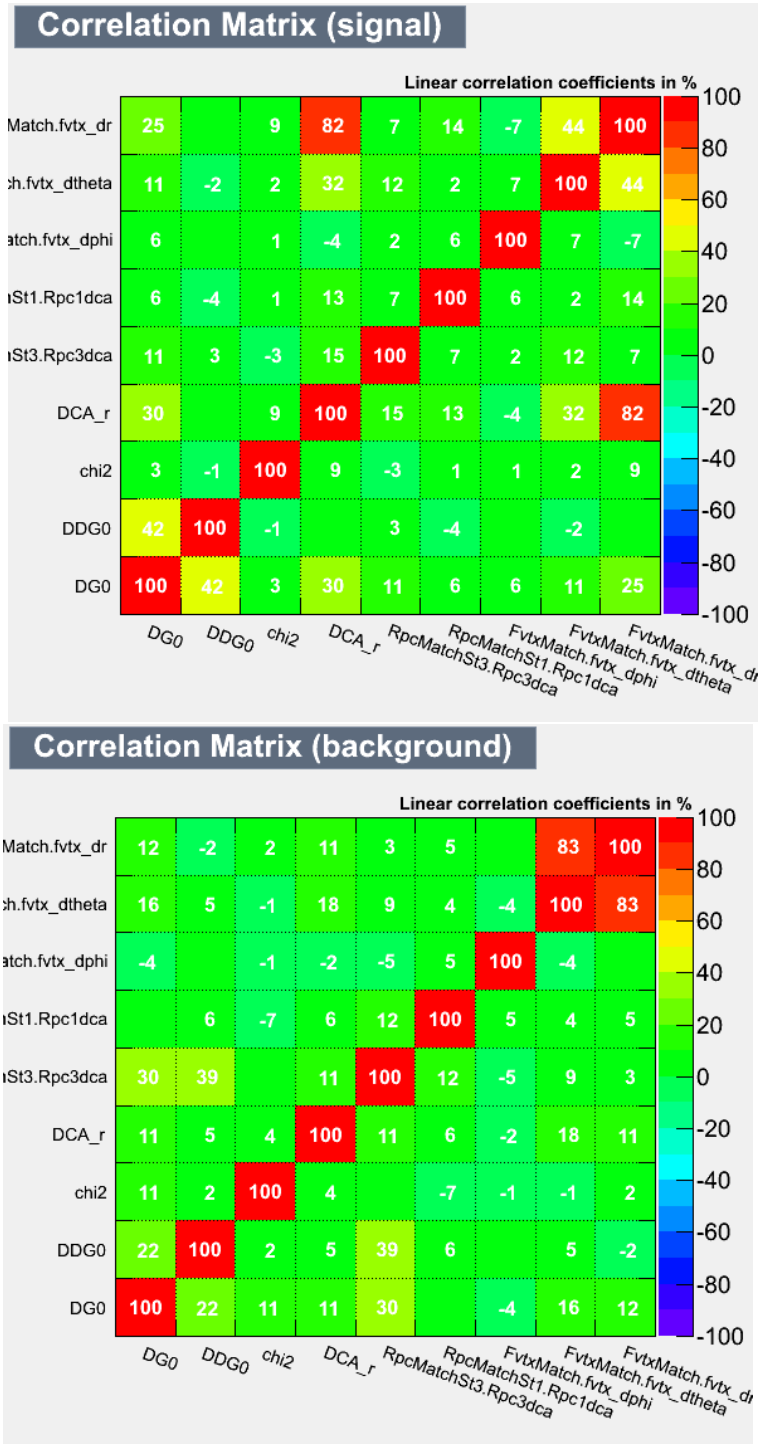

Figure 5.2: Low correlations between the signal variable distributions (from simulation), and the background variable distributions make this data set a good candidate for classfication using Naive Bayes

Briefly, a Naive Bayes classifier may be constructed from the core of the familiar Bayes Theorem from probability and statistics.

In our case, we understand Naive Bayes as a conditional probability. Concretely, we consider a vector of features (i.e. our discriminating kinematic variables):

$$\mathbf{x} = (x_1, \ldots, x_n) \tag{5.1}$$

and assume independence between each feature x_n. We then define the probability of a given classification, C_k given a set of features x_n:

$$p(C_k|x_1, \ldots, x_n) \tag{5.2}$$

This conditional probability is defined in terms of Bayes Theorem:

$$p(C_k|\mathbf{x}) = \frac{p(C_k)\ p(\mathbf{x}|C_k)}{p(\mathbf{x})} \tag{5.3}$$

The terms here are defined as:

- $p(C_k) \rightarrow$ prior probability
- $p(\mathbf{x}|C_k) \rightarrow$ likelihood
- $p(\mathbf{x}) \rightarrow$ evidence

In principal, the final step in a classifier is to assign a class. This is done by computing the probability of a feature-set belonging to one class, or to another class, using Bayes Theroem. The class with the larger proability is than taken as the defacto classification of that particular feature set. However, we may instead observe these probabilities directly, and label data with this probability. This is what we ultimately call our "W_{ness}" parameter. This will be discussed in section **??**.

5.1.2 Composition of Probability Distribution Functions

After we have engineered appropriate features to use in the analysis, we can proceed with composing probability density functions so we can proceed with the calculation of likelihoods, which will label our data set, allowing us to reduce our data set further from the basic cuts, without removing any signal events.

5.1.3 Labeling Data With Likliehood Ratio: W_{ness}

5.2 Extended Unbinned Maximum Likelihood Fits

5.2.1 Modeling The Hadronic Background

5.2.2 Modeling the Muon Background

5.2.3 Modeling the W-Signal

5.2.4 Overview

5.2.5 Fit Performance

5.2.6 S/BG and Muon Backgrounds

5.2.7 W_{ness} Dependence of S/BG

5.3 Data Validation

Mention Daniel's GPR, Ralf's PEPSI, Abraham's FVTX work, and Francesca's cross-checks.

5.3.1 Simulations and The Signal to Background Ratio

5.3.2 Gaussian Process Regression

5.3.3 Four Way Cross Validation

5.3.4 Asymmetry Consistency Check

5.3.5 Beam Polarization

5.3.6 Beam Luminosity

5.3.7 Code Cross Validation

5.4 Calculation of A_L for $W \to \mu$

5.4.1 Overview

5.4.2 Asymmetry Calculation

5.4.3 Discussion of Work Done By Analysis Team

Chapter 6

The Vernier Analysis

6.1 Overview

6.2 Analysis Note Here

6.3 W Cross Section

Chapter 7

Discussion and Conclusion

Bibliography

[1] Bazilevsky A., Bennett R., Deshpande A., and Goto Y. Absolute luminosity determination using the vernier scan technique: Run5-6 analysis and preliminary results at $\sqrt{s} = 62.4gev$. *PHENIX Analysis Note AN688*, 2008.

[2] Bazilevsky A., Bennett R., Deshpande A., Goto Y., Kawall D., and Seele J. Absolute luminosity determination using the vernier scan technique: Run4-6 analysis and preliminary results at $\sqrt{s} = 62.4gev$. *PHENIX Analysis Note AN597*, 2007.

[3] J. Ashman, B. Badelek, G. Baum, J. Beaufays, C. P. Bee, C. Benchouk, I. G. Bird, S. C. Brown, M. C. Caputo, H. W. K. Cheung, J. Chima, J. Ciborowski, R. W. Clifft, G. Coignet, F. Combley, G. Court, G. D'Agostini, J. Drees, M. Düren, N. Dyce, A. W. Edwards, M. Edwards, T. Ernst, M. I. Ferrero, D. Francis, E. Gabathuler, J. Gajewski, R. Gamet, V. Gibson, J. Gillies, P. Graftström, K. Hamacher, D. Von Harrach, P. Hayman, J. R. Holt, V. W. Hughes, A. Jacholkowska, T. Jones, E. M. Kabuss, B. Korzen, U. Krüner, S. Kullander, U. Landgraf, D. Lanske, F. Lettenström, T. Lindqvist, J. Loken, M. Matthews, Y. Mizuno, K. Mönig, F. Montanet, J. Nassalski, T. Niinikoski, P. R. Norton, G. Oakham, R. F. Oppenheim, A. M. Osborne, V. Papavassiliou, N. Pavel, C. Peroni, H. Peschel, R. Piegaia, B. Pietrzyk, U. Pietrzyk, B. Povh, P. Renton, J. M. Rieubland, A. Rijllart, K. Rith, E. Rondio, L. Ropelewski, D. Salmon, A. Sandacz, T. Schröder, K. P. Schüler, K. Schultze, T.-A. Shibata, T. Sloan, A. Staiano, H. Stier, J. Stock, G. N. Taylor, J. C. Thompson, T. Walcher, S. Wheeler, W. S. C. Williams, S. J. Wimpenny, R. Windmolders, W. J. Womersley, K. Ziemons, and European Muon Collaboration. A measurement of the spin asymmetry and determination of the structure function g_1 in deep inelastic muon-proton scattering. *Physics Letters B*, 206:364–370, May 1988.

[4] E. D. Bloom, D. H. Coward, H. DeStaebler, J. Drees, G. Miller, L. W. Mo, R. E. Taylor, M. Breidenbach, J. I. Friedman, G. C. Hartmann, and H. W. Kendall. High-energy inelastic $e - p$ scattering. *Phys. Rev. Lett.*, 23:930–934, Oct 1969.

[5] Michael Collins. The naive bayes model, maximum-likelihood estimation, and the em algorithm.

[6] A. Datta and D. Kawall. σ_{BBC} using vernier scans for 500 *gev* pp data in run09. *PHENIX Analysis Note AN888*, 2010.

[7] A. Drees. Analysis of vernier scans during rhic run-13 (pp at $255gev/beam$). *Collider Accelerator Department (RHIC) AP???*, 2013.

[8] Werner Herr and Bruno Muratori. Concept of luminosity. 2006.

[9] D. Kawall. How to measure absolute luminosity. *PHENIX Focus Seminar*, 2005.

[10] Bogdan Povh and Thomas Walcher. The end of the nucleon-spin crisis. 2016.

[11] Belikov S., Bunce G., Chiu M., Fox B., Goto Y., Kawabata T., Saito N., and Tannenbaum M. Determination of the absolute luminosity for the proton-proton data at $\sqrt{s} = 200gev$ recoreded by phenix during rhic run-02. *PHENIX Analysis Note AN184*, 2002.

[12] R Seidl, H Oide, R Hollis, M Sarsour, J Seele, M Leitgab, Y Imazu, and I Choi. Run 11 w analysis note. *PHENIX Analysis note: AN1024*, 99:403–422, 1992.